Excited Cr impurity states in Al_{2}O_{3} from constraint density functional theory

Y. Kitaoka, K. Nakamura, T. Akiyama, T. Ito, M. Weinert, and A. J. Freeman

Phys. Rev. B **87**, 205113 — Published 10 May 2013

DOI: 10.1103/PhysRevB.87.205113

Excited Cr impurity states in Al_2O_3 from constraint density functional theory

Y. Kitaoka,[1] K. Nakamura,[1,*] T. Akiyama,[1] T. Ito,[1] M. Weinert,[2] and A. J. Freeman[3]

[1]*Department of Physics Engineering,*
Mie University, Tsu, Mie 514-8507, Japan

[2]*Department of Physics, University of Wisconsin-Milwaukee, Milwaukee, Wisconsin 53201*

[3]*Department of Physics and Astronomy,*
Northwestern University, Evanston, Illinois 60208

(Dated: April 17, 2013)

Abstract

The excited states, $^4T_{2g}$ and ^2E_g, of a Cr impurity in Al_2O_3 were treated by constraint density functional theory by imposing a density matrix constraint (constraint field) to control the electron occupation numbers of the d-orbitals. The calculated excitation energies, directly calculated from the self-consistent total energies of the $^4A_{2g}$ ground states and the various excited states, correctly reproduce the experimental ordering. In addition, we find that there is no stationary solution for the excited $^4T_{2g}$ state corresponding to the crystal-field transition state in the usual Kohn-Sham equation, i.e., with no constraint field. By contrast, the excited ^2E_g state of the spin-flip transition state is a (meta-) stable stationary solution, and may be responsible for the long radiative decay lifetime observed in experiments on ruby.

PACS numbers: 71.55.-i, 71.15.Qe

I. INTRODUCTION

State-of-the-art *ab initio* total energy calculations based on density-functional theory (DFT)[1,2] are recognized as a powerful tool for exploring the ground state properties of materials. When extended to electron excitations, the conventional DFT approach of approximating the quasi-particle energies by the Kohn-Sham eigenvalues is often inadequate. Addition and removal energies involving the one-particle excitations require a self-energy correction as demonstrated in GW calculations[3]. Optical spectra typically denoted as two-particle (electron-hole) excitations, where electron remains in the system and interacts with its hole, may be further treated by the Bethe-Salpeter equation that yields the electron-hole interaction[4]. The time-dependent DFT[5] is also used to calculate such optical excitations. However, these approaches are still complex and expensive computationally and may not be appropriate for highly localized electron-systems such as impurity states.

Alternately, the delta self-consistent field (ΔSCF) approach[6] based on the difference in total energies of two states, i.e., ground (G) and excited (E) states, $\Delta E = E(\mathrm{E}) - E(\mathrm{G})$, may provide a satisfactory estimation for all excitations provided that the energies of the two states can be obtained. Another commonly used approach, the Slater transition-state method[6–8], has been successfully applied to excited states in atoms and molecules, and even for the gaps in semiconductors[9,10]. As a practical matter, however, the Slater transition-state method is simply the trapezoidal approximation to the ΔSCF result[8].

A difficulty in applying ΔSCF methods is that the excited states, even when of different symmetry than the ground state, may not be obtainable via conventional self-consistent calculations. To overcome this problem, we perform self-consistent constraint DFT calculations for the excited states by imposing density matrix constraints to control the orbital occupation numbers[11]. Here, we apply our approach to the problem of the highly localized excited Cr impurity states in Al_2O_3 (ruby).

II. STRUCTURE AND EXCITED CR IMPURITY STATES

Cr^{3+} in Al_2O_3 substitutionally occupies cation (Al^{3+}) sites of C_3 symmetry and surrounded by O^{2-} octahedra with a trigonal distortion[12]. This induces sharp $3d$ peaks in the band gap of the host Al_2O_3, Fig. 1(a), exhibiting a crystal field splitting into cubic-like lower

t_{2g} and upper e_g levels; the trigonal distortion results in a further splitting of the t_{2g} into the two irreducible representations, a and e, with a small energy splitting of the order of 0.1 eV[14]. For convenience, we abbreviate these states in the O_h group terminology, t_{2g} ($t_{2g:a}$ and $t_{2g:e}$) and e_g.

From the group theory-based ligand-field study[13], the experimentally observed optical spectrum[14] was described as excitations from the ${}^4A_{2g}$ ground state to the ${}^4T_{2g}$ (U band, 2.23 eV), the ${}^4T_{1g}$ (Y band, 3.01 eV), the ${}^2E_g$ (R line, 1.79 eV), and the ${}^2T_{2g}$ (B line, 2.60 eV) states. The U band and the R line may correspond to the excitations to electronic configurations of $t^2_{2g,\uparrow}e_{g,\uparrow}$ (crystal-field transition) and $t^2_{2g,\uparrow}t_{2g,\downarrow}$ (spin-flip transition), respectively, as shown in Fig. 1(b).

III. MODEL AND METHOD

To model the Cr impurity in Al_2O_3, a supercell containing 80 atoms (corresponds to a 3% Cr) was employed. The atomic positions were fully optimized using the calculated forces, although the experimental lattice constants of Al_2O_3 were employed for a computational simplicity to demonstrate the large system for narrow impurity levels. The calculated interatomic distances of the nearest and second-nearest neighbors between the Cr and O atoms, 1.95 Å and 1.99 Å in the local-spin-density approximation (LSDA) agree well with experimental values of 1.92 and 2.01 Å[12], respectively. No difference in the calculated equilibrium geometry in the LSDA+U was confirmed. The calculations were performed using the full-potential linearized augmented plane-wave (FLAPW) method[15,16].

To constrain an electronic configuration of a given excited state without loss of site symmetry, we introduce an appropriate functional with constraint fields[11]:

$$E[\rho(\mathbf{r})] = E_{\mathrm{LSDA}}[\rho(\mathbf{r})] + \sum_{mm'} \mu^{\alpha}_{m'm}(n^{\alpha}_{mm'} - N^{\alpha}_{mm'}), \tag{1}$$

where $E_{\mathrm{LSDA}}[\rho(\mathbf{r})]$ is the usual total energy functional such as the LSDA, $n^{\alpha}_{mm'}$ is the density matrix of d-orbitals of atom α, and $N^{\alpha}_{mm'}$ is the occupation number that should be constrained. In the LAPW basis, $n^{\alpha}_{mm'}$ is given by the projection of the wave function onto the $Y_{\ell m}$ subspace[17] as

$$n^{\alpha}_{mm'} = \sum_{\mathbf{k},b} f_{\mathbf{k},b} \langle \Phi_{\mathbf{k},b} \, | \hat{\mathrm{P}}^{\alpha}_{mm'} | \, \Phi_{\mathbf{k},b} \rangle, \tag{2}$$

$$\hat{\mathrm{P}}^{\alpha}_{mm'} = |u^{\alpha}_{\ell} Y_{\ell m}\rangle\langle u^{\alpha}_{\ell} Y_{\ell m'}| + \frac{1}{\langle \dot{u}_{\ell}\dot{u}_{\ell}\rangle}|\dot{u}^{\alpha}_{\ell} Y_{\ell m}\rangle\langle \dot{u}^{\alpha}_{\ell} Y_{\ell m'}|, \tag{3}$$

where $\mathbf{k}$ and b refer to a $\mathbf{k}$-point in the Brillouin zone and a band index, respectively. The corresponding Kohn-Sham equation can be written as

$$\left[H_{\mathrm{LSDA}} + \sum_{mm'} \mu^{\alpha}_{m'm} \hat{\mathrm{P}}^{\alpha}_{mm'} \right] \Phi_{\mathbf{k},b} = \epsilon \Phi_{\mathbf{k},b}. \tag{4}$$

The constraint term in the Hamiltonian effectively projects out the chosen irreducible representation from the overall wave function, thus allowing one to pick up the electronic configuration corresponding to the excited state.

In practice, we specify a set of constraint fields, μ^{α}_{n}, along the directions of the eigenvectors of $n^{\alpha}_{mm'}$, consistent with the site symmetry ($\mu_{t_{2g}:a}$, $\mu_{t_{2g}:e}$, and μ_{e_g} in the case of the C_3 symmetry). Then, the $\mu^{\alpha}_{mm'}$, which are rotated back from the μ^{α}_{n}, are introduced into Eq. 4, and the corresponding $n^{\alpha}_{mm'}$ are determined self-consistently. The self-consistent calculations were carried out using the second-variation scheme, i.e., the diagonalization of Eq. 4 was carried out in a basis of the eigenfunctions, $\phi_{\mathbf{k},b}$, of H_{LSDA}. Full self-consistency was achieved for the density matrix as well as the charge and spin densities. The total energy is calculated using Eq. 1, with $N^{\alpha}_{mm'} = n^{\alpha}_{mm'}$.

IV. RESULTS AND DISCUSSION

We first present the Kohn-Sham eigenstates for the ground state of the Cr impurity in Al_2O_3. The calculated density of states (DOS) in the LSDA[18] is shown in Fig. 2(a). The LSDA calculations clearly demonstrate sharp Cr impurity levels in the energy gap between the valence and conduction bands. The fully occupied majority-spin $t^3_{2g,\uparrow}$ states are located at 1.7 eV above the valence band maximum. The eigenvalue difference between the highest occupied and lowest unoccupied orbital states for the $e_{g,\uparrow}$ and $t_{2g,\downarrow}$, are 2.5 and 2.2 eV, respectively, in surprisingly good agreement with the experimental optical spectrum, 2.23 and 1.79 eV for the $^4T_{2g}$ and ^2E_g states[14].

The Kohn-Sham eigenvalues, which differ from an analog of Koopmans' theorem, have somewhat unclear physical meaning; for example, they need to be corrected for the derivative discontinuity in the exchange-correlation potential[19,20]. Accidental agreement with the experiments above may be involved, as a result of the cancellation effect due to the insufficiency of the LSDA correlation and no electron-hole relaxation. Moreover, recent LSDA+U

calculations[21] and combined DFT calculations with the configuration interaction method[22] pointed out the importance of electron correlation effects in the localized Cr $3d$-orbitals in ruby. Even in the case of pure Cr_2O_3, which has less localized character compared to the impurity states, the LSDA+U calculations give great improvements for structural ground-state properties of the bulk and at surfaces[23–25].

We thus carried out LSDA+U calculations[17,26] using literature U and J parameters (4.0 eV and 0.58 eV, respectively) of Cr_2O_3[23,24]. The calculated DOS is shown in Fig. 2(b). Although the energy gap arising from the Al_2O_3, about 5.9 eV, remains to underestimate compared to that in experiments, 8.9 eV[27], the localized feature of the Cr impurity state is well demonstrated. In general, eigenvalues in the LSDA+U show a better agreement with one-particle excitation energies than the LSDA eigenvalues. In the present calculations, the occupied $t_{2g,\uparrow}$ state is pushed down in energy to near the top of the valence band, and the separation between the occupied $t_{2g,\uparrow}$ and unoccupied $e_{g,\uparrow}$ states is increased compared to those in the LSDA. The eigenvalue differences are now 4.2 and 4.6 eV, respectively, which are significantly larger than those in the LSDA.

We now consider constraint DFT calculations for the excited $^4T_{2g}$ and ^2E_g states, the results in the LSDA and LSDA+U are shown in Fig. 3. For the $^4T_{2g}$ state, a set of constraint fields ($\mu_{t_{2g:a},\uparrow}$=$\mu_\downarrow$=5.4 eV, where $\mu_\downarrow$ is used for all minority-spin d-states) was initially introduced[11]. A series of self-consistent calculations in which the μ_n's were gradually set back to zero (zero constraint field, corresponding to the standard LSDA/LSDA+U solution) are illustrated in the figures. At zero constraint field in both LSDA and LSDA+U, we could not obtain a solution for the $^4T_{2g}$ electronic configuration; instead, the system always iterated back to the ground $^4A_{2g}$ state. Thus, there is no stationary solution in the standard LSDA/LSDA+U; the lowest constraint fields at $\mu_{t_{2g:a},\uparrow}$=$\mu_\downarrow$= 3.8 eV in the LSDA and 2.7 eV in the LSDA+U that allowed a stationary state yields an energy for this excited state of 3.0 and 3.1 eV, respectively, both overestimate the experimental value of 2.23 eV[14].

However, an extrapolation to zero field, as illustrated by a dashed line in Fig. 3, is close to the experimental value, where the trends in the LSDA and LSDA+U results are similar. A lifting of the degeneracy in the excited state, where the either of the doublet $e_{g,\uparrow}$ is occupied by one electron [cf., Fig. 1(b)], may reduce the total energy of the excited state by a Jahn-Teller effect[28,29]. It notes that the excited energy is lower than that in the eigenvalue difference of the LSDA+U, which demonstrates an electron-hole relaxation.

For the ^2E_g case, starting with constraint fields of $\mu_{t_{2g:a},\downarrow}$=−5.4 eV, the system is found to remain in a stationary solution at zero constraint field in both LSDA and LSDA+U; the state is (meta-) stable, which, together with the low probability of spin-flip transitions, may lead to the long radiative decay lifetime and provide a sharp optical spectrum, as observed in experiments[30]. The calculated energy, 1.1 eV in the LSDA and 0.9 eV in the LSDA+U, underestimates the experimental value of 1.79 eV[14]. Although more theoretical effort is needed for a quantitative prediction, $\Delta E(^2E_g) < \Delta E(^4T_{2g})$, which reproduces the correct ordering of the optical energy levels in the experiments.

The calculated d-electron occupations in the Cr muffin-tin sphere ($R_{\rm MT}$ = 1.16 Å) for the $^4A_{2g}$ ground state, and the $^4T_{2g}$ and ^2E_g excited states in the LSDA and LSDA+U are summarized in Table I. The results clearly demonstrate that electrons in the $t_{2g,\uparrow}$ orbital in the ground $^4A_{2g}$ state are transferred to the $e_{g,\uparrow}$ orbital for the $^4T_{2g}$ state, and to the $t_{2g,\downarrow}$ orbital for the ^2E_g state. Moreover, the charge difference in the excited and ground states, $\Delta\rho(\mathbf{r}) = \rho_{\rm E}(\mathbf{r}) - \rho_{\rm G}(\mathbf{r})$, shown in Fig. 4, indicates that for the $^4T_{2g}$ state, the charge accumulation (corresponding to the excited electrons) and depletion (holes) appear only around the Cr impurity site. In contrast, for the ^2E_g case, almost no change in the charge difference is observed (not shown) since the spin-flip excitation does not alter the charge distribution.

V. SUMMARY

We have performed constraint DFT total energy calculations to estimate total energy differences between the ground and excited states, for the optical excitations of the Cr impurity states in Al_2O_3. Results demonstrate that the excited energies of the $^4T_{2g}$ and ^2E_g states, corresponding to the crystal-field and spin-flip transition states, are 2.8 and 1.1 eV in the LSDA, and 3.1 and 0.9 eV in the LSDA+U, which reproduce the correct experimental ordering of the excited energy levels. For the excited $^4T_{2g}$ state, there is no stationary solution in zero constraint field in both LSDA and LSDA+U. By contrast, the excited ^2E_g state is metastable against electron density variations, which may lead to the long radiative decay lifetime observed in experiments. The excited electron and hole densities in the $^4T_{2g}$ state appears only around the Cr impurity site, while in the ^2E_g state, no charge redistribution from the ground state is observed.

Acknowledgements

We thank Prof. T. Oguchi for fruitful discussions. Work at Mie University was supported by a Grant-in-Aid for Scientific Research (No. 24540344) and Young Researcher Overseas Visits Program for Vitalizing Brain Circulation (R2214) from the Japan Society for the Promotion of Science, and was performed under the Cooperative Research Program of "Network Joint Research Center for Materials and Devices". Computations were partially performed at ISSP, University of Tokyo. Work at Northwestern University was supported by the U.S. Department of Energy (DE-FG02-88ER45372) and at the University of Wisconsin-Milwaukee by the National Science Foundation (DMR-1105839).

* Email address: kohji@phen.mie-u.ac.jp

[1] P. Hohenberg and W. Kohn, Phys. Rev. **136**, B864 (1964).

[2] W. Kohn and L. J. Sham, Phys. Rev. **140**, A1133 (1965).

[3] L. Hedin, Phys. Rev. **139**, A796 (1965).

[4] G. Onida, L. Reining, A. Rubio, Rev. Mod. Phys. **74**, 601 (2002).

[5] E. Runge and E. K. U. Gross, Phys. Rev. Lett. **52**, 997, (1984).

[6] R. M. Martin, *Electronic Structure: Basic Theory and Practical Methods* (Cambridge University Press, Cambridge, England, 2004)

[7] J. C. Slater and K. H. Johnson, Phys. Rev. B **5**, 844 (1972); J. C. Slater, Adv. Quantum Chem. **6**, 1 (1972).

[8] J. F. Janak, Phys. Rev. B 18, 7165 (1978).

[9] D. A. Liberman, Phys. Rev. B **62**, 6851 (2000).

[10] L. G. Ferreira, M. Marques, and L. K. Teles, Phys. Rev. B **78**, 125116 (2008).

[11] K. Nakamura, Y. Kitaoka, T. Akiyama, T. Ito, M. Weinert, and A. J. Freeman, Phys. Rev. B., Phys. Revie. B **85**, 235129, (2012).

[12] L. W. Finger and R. M. Hazen, J. Appl. Phys. **51**, 5362 (1980).

[13] S. Sugano and Y. Tanabe, J. Phys. Soc. Jpn. **13**, 880 (1958).

[14] W. M. Fairbank Jr., G. K. Klauminzer, and A. L. Schawlow, Phys. Rev. B **11**, 60 (1975).

[15] E. Wimmer, H. Krakauer, M. Weinert, and A. J. Freeman, Phys. Rev B **24**, 864 (1981).

[16] M. Weinert, E. Wimmer, and A. J. Freeman, Phys. Rev. B **26**, 4571 (1982).

[17] A. B. Shick, A. I. Liechtenstein, and W. E. Pickett, Phys. Rev. B **60**, 10763 (1999).

[18] U. von Barth and L. Hedin, J. Phys. C **5**, 1629 (1972).

[19] C. S. Wang and W. E. Pickett, Phys. Rev. Lett. **51**, 597 (1983).

[20] L. J. Sham and M. Schluter, Phys.Rev. Lett. **51**, 1888 (1983).

[21] V. V. Mazurenkoa, A. N. Varaksina, V. G. Mazurenkoa, V. S. Kortova, and V. I. Anisimov Physica B **344** 385 (2004).

[22] K. Ogasawara, T. Ishii, I. Tanaka, H. Adachi, Phys. Rev. B **61**, 143 (2000).

[23] A. Rohrbach, J. Hafner and G. Kresse, Phys. Rev. B **70**, 125426 (2004).

[24] S. Shi, A. L. Wysocki and K. D. Belashchenko, Phys. Rev. B **79**, 104404 (2009).

[25] N. J. Mosey, E. A. Carter, Phys. Rev. B **76**, 155123 (2007).

[26] V. I. Anisimov, F. Aryasetiawan, and A. I. Liechtenstein, J. Phys: Condens. Matter **9**, 767 (1997).

[27] R. W. Grimes, J. Am. Ceram. Soc. **77**, 378 (1994).

[28] M. D. Sturge, Phys. Rev. **140**, A880 (1965).

[29] K. Bellafrouh, C. Daul, H. U. Güdel, F. Gilardoni, and J. Weber, Heor. Chim Acta **91**, 215 (1995).

[30] D. F. Nelson and M. D. Sturge, Phys. Rev. **137**, A1117 (1965).

Figures

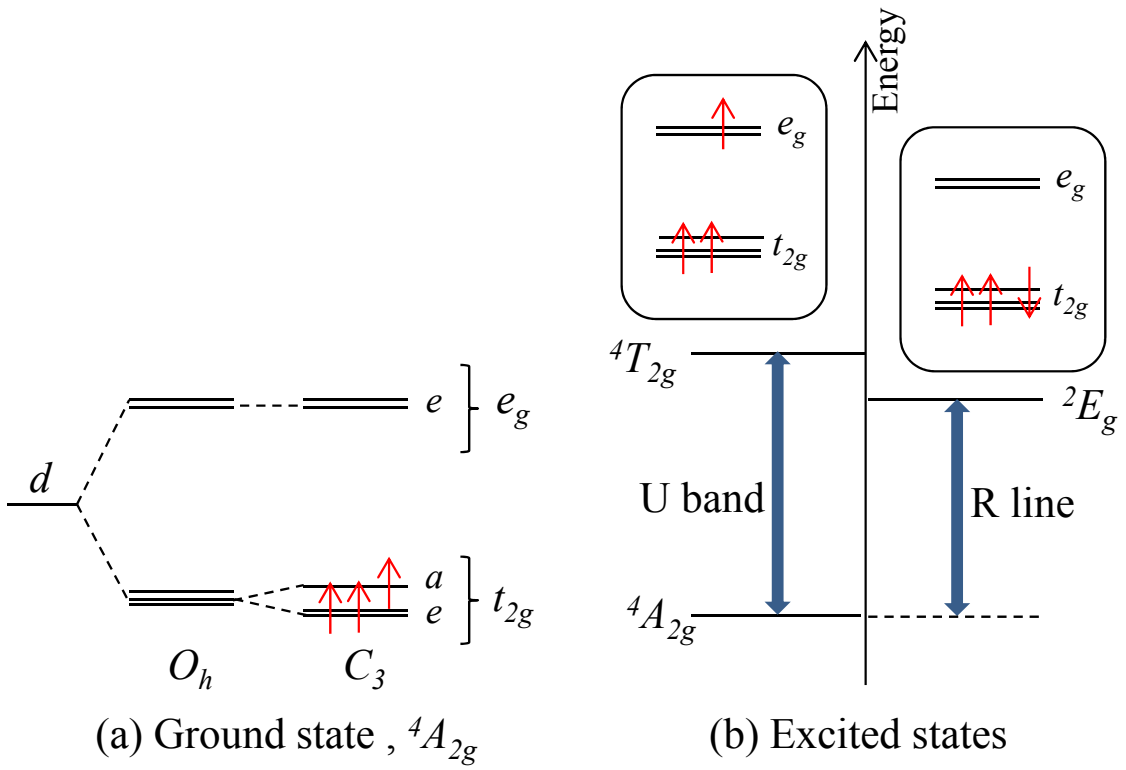

FIG. 1: (Color online) (a) Schematic electronic structure of the $^4A_{2g}$ ground state of a Cr impurity with a C_3 site symmetry in Al_2O_3, exhibiting cubic-like O_h splitting into lower t_{2g} and upper e_g levels, which under the trigonal distortion split into a and e irreducible representations. (b) two-particle excitations from the ground $^4A_{2g}$ state to $^4T_{2g}$ (U band) and ^2E_g (R line) states, which correspond to the electronic configurations $t^2_{2g,\uparrow}e_{g,\uparrow}$ and $t^2_{2g,\uparrow}t_{2g,\downarrow}$, respectively.

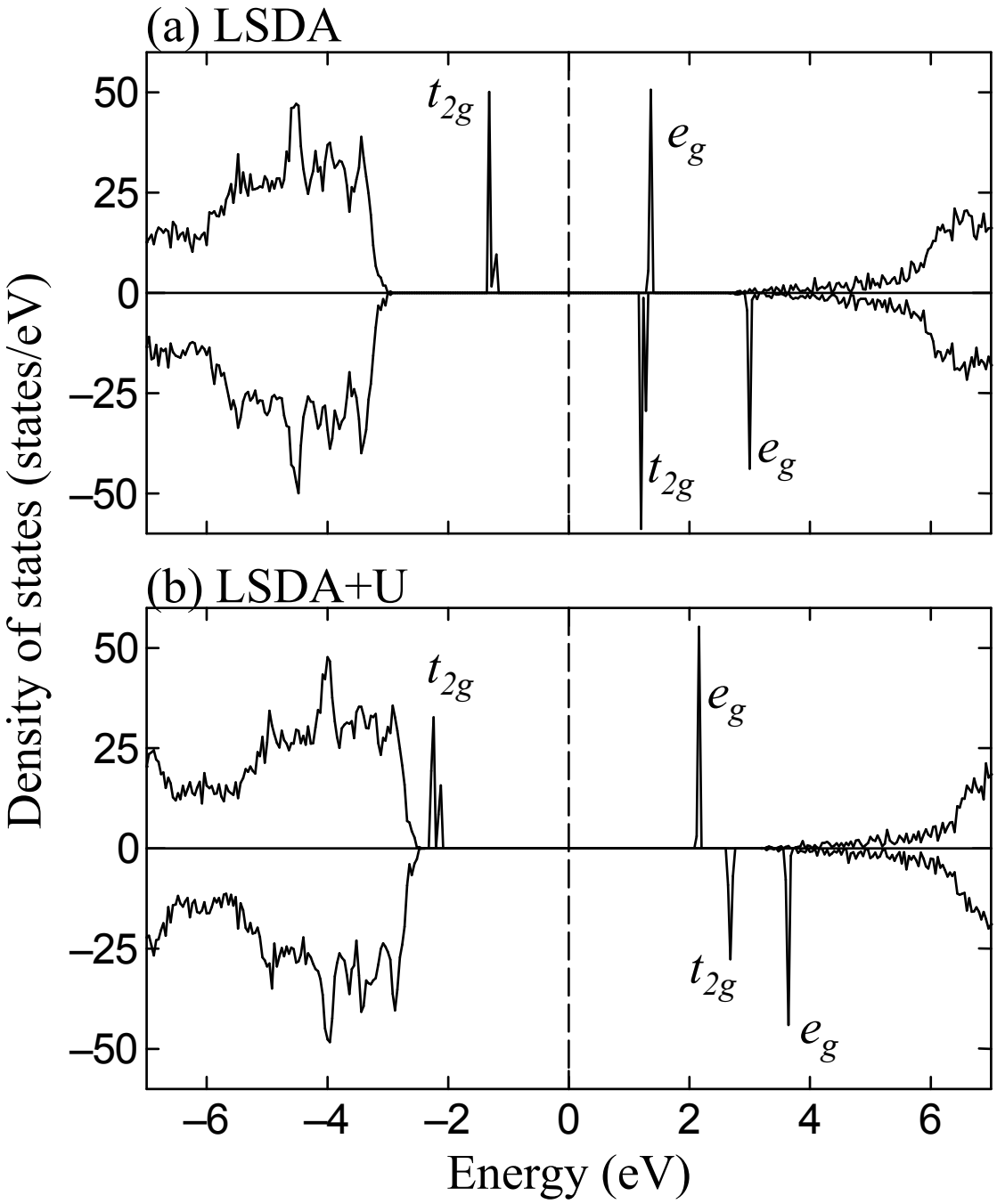

FIG. 2: Density of states (DOS) for Al_2O_3:Cr^{3+} in (a) LSDA and (b) LSDA+U for U=4.0 eV and J=0.58 eV; zero energy corresponds to the Fermi level. The narrow peaks in the plots correspond to the Cr d impurity states.

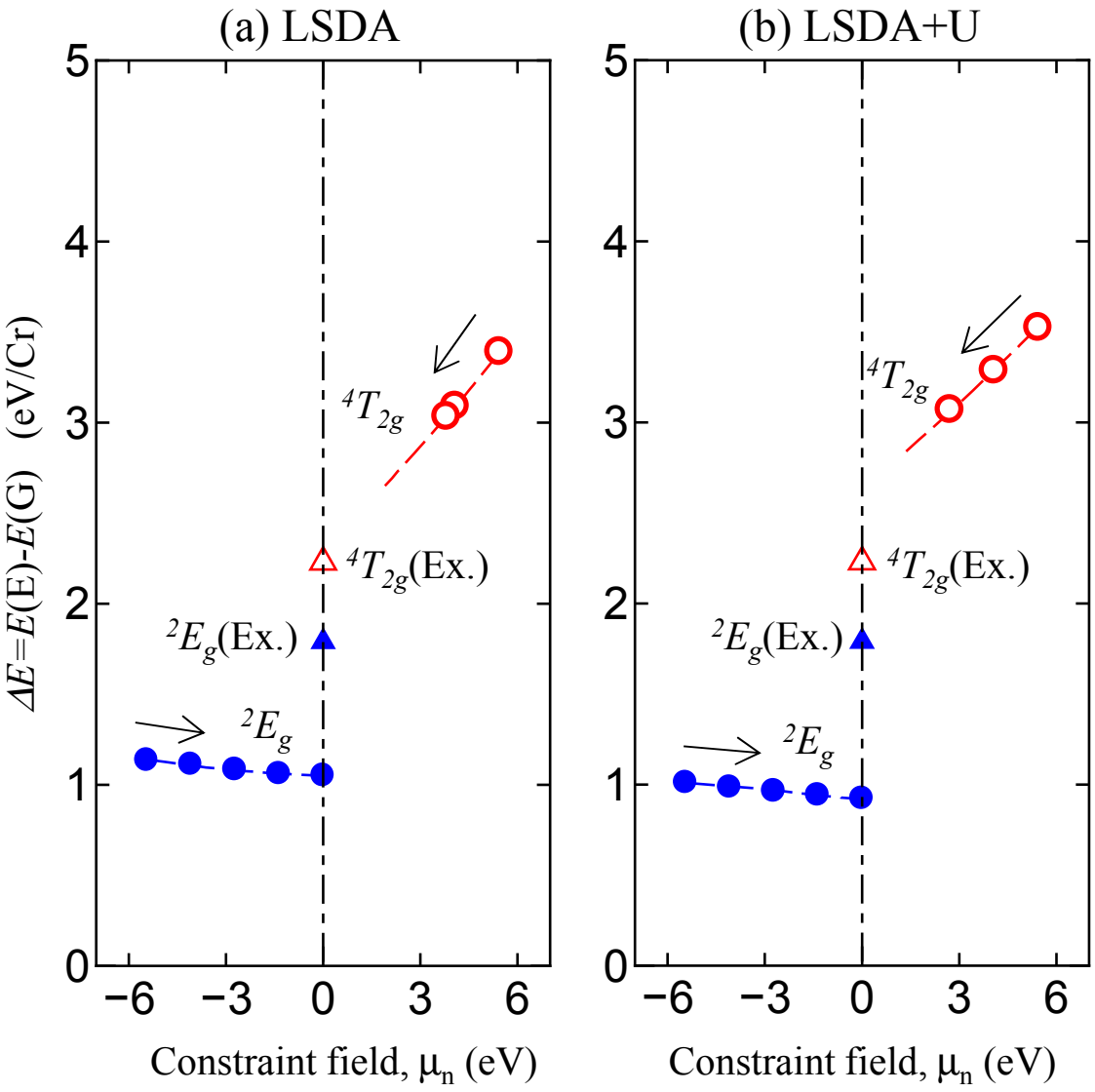

FIG. 3: (Color online) Calculated total energy differences, ΔE, of the excited $^4T_{2g}$ and ^2E_g states with respect to $^4A_{2g}$ ground state, in (a) LDSA and (b) LSDA+U, as a function of the constraint field, μ_n, for a Cr impurity in Al_2O_3. Calculations were started with a set of constraint fields and then all μ_ns were gradually set back to zero. For the $^4T_{2g}$ state, there is no stationary solution at zero constraint field. Triangles represent those in experiments (Ex).

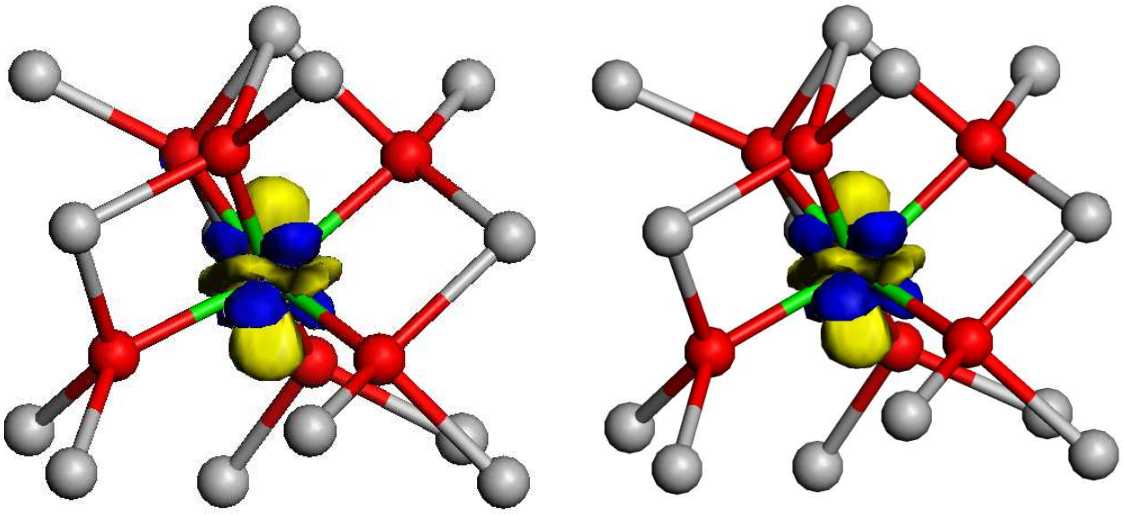

(a) LSDA (b) LSDA+U

FIG. 4: (Color online) Calculated charge density difference, $\Delta\rho(\mathbf{r}) = \rho_{\mathrm{E}}(\mathbf{r}) - \rho_{\mathrm{G}}(\mathbf{r})$, between the ${}^4T_{2g}$ excited state and the ground state of a Cr impurity in Al_2O_3 in (a) LSDA and (b) LSDA+U. Dark (blue) and light (yellow) contour planes represent positive (excited electron) and negative (hole) values of the charge difference, 1.4×10^{-2} electrons/bohr^3. Oxygen and aluminum ions are represented by red and gray circles, respectively, and chromium ions are located in the center.

Tables

TABLE I: Calculated electron occupations of the d-orbitals in the Cr MT sphere for the $^4A_{2g}$ ground state, and the $^4T_{2g}$ and ^2E_g excited states. Results for the $^4T_{2g}$ state are obtained at a constraint field of $\mu_{t_{2g:a},\uparrow}$=$\mu_\downarrow$= 3.8 eV in LSDA and 2.7 eV in LSDA+U.

	$^4A_{2g}$[G]		$^4T_{2g}$[E]		^2E_g[E]	
	LSDA	+U	LSDA	+U	LSDA	+U
$e_{g,\uparrow}$	0.57	0.52	1.35	1.38	0.52	0.48
$t_{2g,\uparrow}$	2.69	2.73	1.90	1.93	1.82	1.87
$e_{g,\downarrow}$	0.12	0.09	0.07	0.06	0.14	0.10
$t_{2g,\downarrow}$	0.48	0.44	0.34	0.32	1.35	1.34